Energies of high-n barium Rydberg states

J. Neukammer,* G. Jönsson,† A. König, K. Vietzke,‡ H. Hieronymus, and H. Rinneberg*
Freie Universität Berlin, Institut für Atom- und Festkörperphysik, Arnimallee 14, D-1000 Berlin 33, West Germany
(Received 18 April 1988)

We have measured the energies E_n of $6sns\ ^1S_0$ $(30 \le n \le 214)$, $6snp\ ^1P_1$ $(60 \le n \le 214)$, and $6snd\ ^1D_2$ $(30 \le n \le 285)$ Rydberg states of barium with an accuracy of ± 60 MHz. For the $^1D_2$ series the energy separations $E_{n+1} - E_n$ between neighboring Rydberg states have been deduced with an uncertainty of ± 10 MHz. The singlet-triplet splitting between $6snd\ ^1D_2$ and $^3D_2$ states is reported for principal quantum numbers ranging between $n = 30$ and $n = 190$. In addition, we have determined the energies of $6snf\ ^1F_3$, $6sng\ ^1G_4$, $6sng\ ^3G$, and $6snh\ ^1H_5$ Rydberg states at lower principal quantum numbers $(47 \le n \le 78)$. From our measurements we have deduced quantum defects δ_l of the corresponding $6snl\ ^1L_l$ Rydberg series to be $\delta_0(n \ge 50) = 4.212(5)$, $\delta_1(n \ge 100) = 4.332(5)$, $\delta_2(n \ge 78) = 2.718(5)$, $\delta_3(47 \le n \le 78) = 0.047(5)$, $\delta_4(47 \le n \le 78) = 0.059(5)$, and $\delta_5(47 \le n \le 78) = 0.019(5)$. The first ionization limit of barium has been determined to be $I_{6s} = 42\,034.902(3)\ \mathrm{cm}^{-1}$.

Within the last ten years, Rydberg states of barium have been studied extensively. In particular, experimental and theoretical investigations aimed at analyzing perturbations of $6snl$ Ba Rydberg series caused by configuration interactions with doubly excited states. Such perturbations may result in pronounced deviations from the regular scaling of atomic properties of Rydberg states with principal quantum number n. Energies of Rydberg states,[1–9] lifetimes,[10–14] isotope shifts, and hyperfine structures[15–29] have been analyzed to gain quantitative information on configuration interactions. In addition, the behavior of Ba Rydberg states in external electric[30–33] and magnetic[34–36] fields has been studied to this end. Multichannel quantum defect theory has been frequently applied to analyze such data, a subject covered by several review articles.[37–40]

More recently, spectra of barium Rydberg states with high principal quantum numbers ($n > 100$) have been reported.[41,42] Such highly excited states are readily perturbed by small external electric and magnetic fields. The distribution of oscillator strength across Stark and diamagnetic manifolds of barium Rydberg states in electric, magnetic, and combined fields has been studied recently.[41,43,44] In the l-mixing region the distribution of oscillator strength is strongly influenced by the presence of core penetrating, low angular momentum states. In order to account for these effects, quantitatively, energies of high-n barium Rydberg states in zero field have to be known precisely. In this paper we report energies of $6snl\ ^{1,3}L_l$ Ba Rydberg states with an accuracy of ± 60 MHz. The data have been obtained using high-resolution laser spectroscopy. Our measurements either extend previous data to higher principal quantum numbers or are of improved precision.

We have populated Rydberg states of barium employing the excitation schemes shown in Fig. 1. Starting from the $6s^2\ ^1S_0$ ground state, $6sns\ ^1S_0$ and $6snd\ ^{1,3}D_2$ Rydberg states were reached via the $6s6p\ ^1P_1$ intermediate level [Fig. 1(a)]. Stark mixing of Rydberg states caused by small external electric fields allowed us to obtain energies of $6snp\ ^1P_1$ levels. The excitation scheme shown in Fig. 1(b) served to reach $6snd\ ^{1,3}D_2$ and $6sng\ ^{1,3}G$ Rydberg states. The metastable state $5d6s\ ^1D_2$ was populated by a dc discharge. Again, Stark mixing was employed to excite odd parity $6snf\ ^1F_3$ and $6snh\ ^1H_5$ states via the $5d6p\ ^1F_3$ intermediate level. An atomic beam apparatus [Fig. 2(a)] was used in these experiments. The third excitation scheme [Fig. 1(c)] served for a measurement of the frequency separation between neighboring $6s(n+4)p\ ^1P_1$ and $6snf\ ^1F_3$ Rydberg states. In order to compensate for the low oscillator strength of the electric quadrupole transition to the $5d^2\ ^3P_2$ intermediate state, this experiment was performed in a vapor cell [Fig. 2(b)].

Two counterpropagating, linearly polarized cw dye lasers, stabilized to a bandwidth of about 1 MHz intersected an atomic beam [Fig. 2(a)] at 90°. The collimation ratio of the atomic beam was about 1:150. For the first and second transition of the excitation scheme shown in

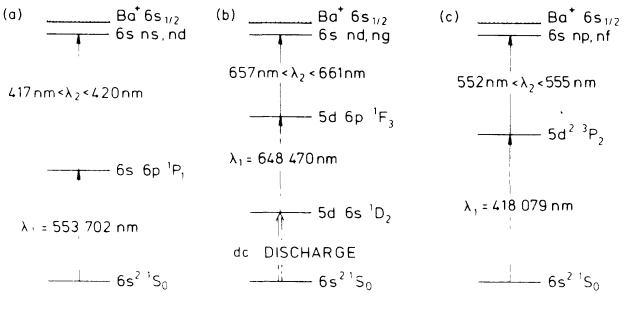

FIG. 1. Excitation schemes used to populate $6snl$ Rydberg states of barium in an atomic beam (a),(b) and a vapor cell (c). An electric quadrupole transition ($E2$) serves as first step in scheme (c).

Fig. 1(a) we used Rhodamine 110 (Lambdachrome 5700) and Stilbene 3 (Lambdachrome 4200) as laser dyes, respectively. The second excitation scheme [Fig. 1(b)] required the dye DCM (Lambdachrome 6500) for both lasers. All dyes were purchased from Lambda Physik, Göttingen, West Germany. The excitation region was shielded from stray electric fields by means of a parallel-plate capacitor. In addition, this capacitor was used to apply electric fields along the atomic beam axis. An electrostatic lens focused the ions onto the entrance aperture of a quadrupole mass filter, which was used to suppress background ions. The vapor cell [Fig. 2(b)] consisted of a stainless steel tube, filled with Ba and heated to about 650 °C. To prevent coating of the windows, the pipe was filled with about 5×10^{-2} Torr of Ar buffer gas. For thermionic detection[45,46] the stainless-steel pipe was taken as anode while 12 tungsten wires in an annular arrangement served as cathode. The voltage drop across a 50-kΩ load resistor was fed into a lockin amplifier. The first and second dye lasers were operated with Stilbene 3 and Rhodamine 110 as dyes [Fig. 1(c)], respectively. Both laser beams were superimposed and counterpropagated through the vapor cell.

The Rydberg atoms, excited in the atomic beam, were ionized by different mechanisms. At principal quantum numbers $n>30$ the kinetic energy which can be transferred in forward collisions with Ba ground state atoms is sufficient to ionize the Rydberg atoms. Recently, Penning ionization of $6sns\ ^1S_0$ ($14\le n\le 50$) Rydberg atoms has been studied[47] by analyzing the kinetic energy of the emitted electrons. Barium atoms predominantly in $6s6p\ ^1P_1$ or $5d6s\ ^1D_2$ states served as collision partners. Furthermore, field ionization of the Rydberg states may occur for $n>60$. Above $n=60$, the radiative lifetimes were sufficiently long for the Rydberg atoms to leave the parallel plate capacitor. Subsequently, these atoms were ionized by the electric field caused by the potential difference between the first electrode of the einzel lens and the upper capacitor plate. A field strength of about 25 V/cm is sufficient to ionize Rydberg states with $n\approx60$. In a thermionic diode collisions with Ba atoms in their ground state as well as Penning ionization are expected to contribute to the ionization of Rydberg atoms. In addition, associative ionization between barium ground state atoms and Rydberg atoms may occur because of the rather high barium vapor pressure. Furthermore, collisions of Rydberg atoms with buffer gas atoms may result in the production of Ba^+ ions. The contributions of the various processes to the observed signal depend on the system under study and are poorly understood.

Spectra were recorded by scanning the frequency Ω_2 of the second dye laser across the upper atomic transition, while the other dye laser was stabilized to the wavelength λ_1 of the first transition. For selected $6sns\ ^1S_0$ and

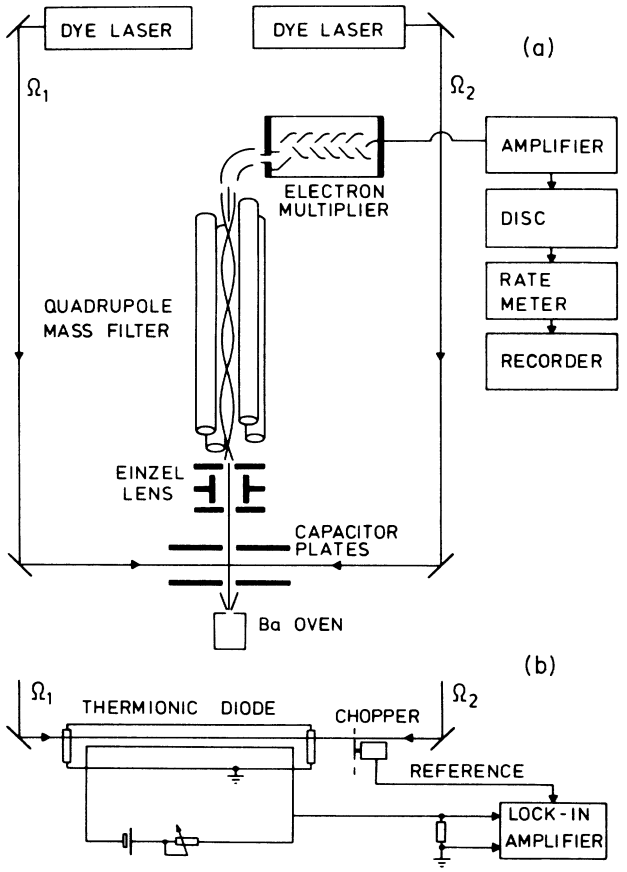

FIG. 2. Experimental setups used to excite Ba Rydberg states in an atomic beam (a) or a vapor cell (b). The corresponding excitation schemes are shown in Figs. 1(a), 1(b), and 1(c), respectively. The abbreviation "disc." stands for discriminator.

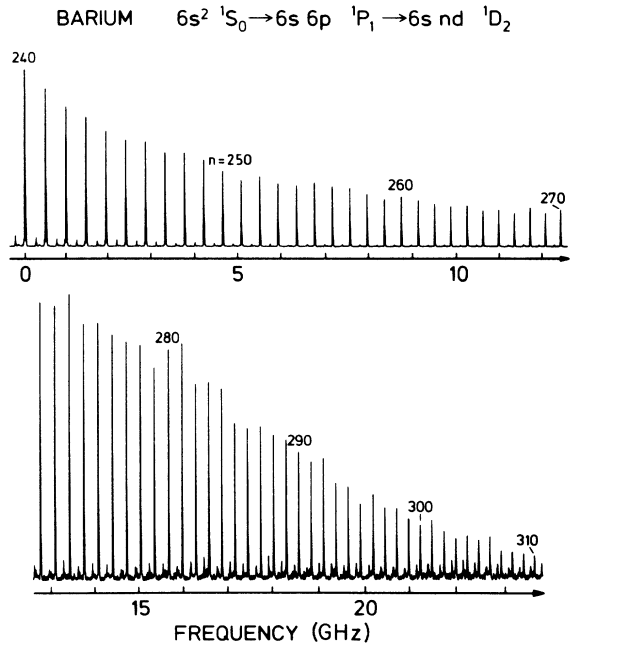

FIG. 3. Spectrum of $6snd\ ^1D_2$ ($240\le n\le310$) Ba Rydberg states. The small signals which appear in the upper trace correspond to $6sns\ ^1S_0$ states. The origin of the frequency scale coincides with the energy of the $6s240d\ ^1D_2$ Rydberg state (see Table I).

TABLE I. Energies of $6snd\ ^1D_2$ Rydberg states of barium ($30 \leq n \leq 285$) with respect to the atomic ground state. The energies were measured using a high-precision Michelson interferometer except those marked by an asterisk, which were interpolated using a marker cavity. The overall uncertainty amounts to $\pm 0.002\ cm^{-1}$. In addition, the differences $E_{n+1}-E_n$ between the energies of neighboring Rydberg states are given with an uncertainty of ± 10 MHz. Values in parentheses are less accurate by an order of magnitude.

n	Energy (cm^{-1})	$E_{n+1}-E_n$ (MHz)	n	Energy (cm^{-1})	$E_{n+1}-E_n$ (MHz)	n	Energy (cm^{-1})	$E_{n+1}-E_n$ (MHz)	n	Energy (cm^{-1})	$E_{n+1}-E_n$ (MHz)
30	41887.998		125*	42027.564	3550	179*	42031.372	1188	233*	42032.832	533
38	41946.842		126*	42027.682	3462	180	42031.412	1175	234*	42032.850	530
50	41985.833		127*	42027.796	3401	181*	42031.451	1150	235*	42032.868	521
60	42001.465		128*	42027.911	3307	182*	42031.490	1133	236*	42032.885	516
65	42006.617		129	42028.020	3225	183*	42031.527	1110	237*	42032.902	509
70	42010.663		130*	42028.128	3154	184	42031.564	1098	238*	42032.919	498
75	42013.900		131*	42028.233	3077	185*	42031.601	1073	239*	42032.936	497
78	42015.542	(15110)	132*	42028.335	3015	186*	42031.636	1055	240*	42032.952	490
79	42016.046	(14420)	133*	42028.436	2940	187*	42031.672	1041	241*	42032.969	487
80	42016.527	(14030)	134	42028.534	2879	188*	42031.706	1026	242*	42032.985	482
81	42016.995	(13431)	135*	42028.630	2809	189*	42031.741	1006	243*	42033.001	473
82	42017.443	(12981)	136*	42028.724	2745	190*	42031.774	988	244*	42033.017	463
83	42017.876	(12501)	137*	42028.815	2680	191*	42031.807	975	245*	42033.032	459
84	42018.293	(11992)	138	42028.906	2626	192*	42031.840	959	246*	42033.048	459
85	42018.693	(11602)	139*	42028.994	2567	193*	42031.872	942	247*	42033.063	448
86	42019.080	(11212)	140*	42029.079	2523	194*	42031.903	925	248*	42033.078	444
87	42019.454	(10823)	141	42029.165	2463	195	42031.934	910	249*	42033.093	438
88	42019.815	(10343)	142*	42029.247	2408	196*	42031.964	893	250*	42033.107	430
89	42020.160	(10133)	143*	42029.327	2360	197*	42031.994	884	251*	42033.122	430
90	42020.498	(9707)	144	42029.404	2306	198*	42032.024	877	252*	42033.136	416
91	42020.822	(9384)	145*	42029.481	2263	199*	42032.053	868	253*	42033.150	417
92	42021.135	(9113)	146*	42029.556	2222	200*	42032.082	846	254*	42033.164	414
93	42021.439	(8691)	147*	42029.631	2158	201*	42032.110	839	255*	42033.177	405
94	42021.729	(8604)	148*	42029.703	2120	202*	42032.138	825	256*	42033.191	400
95	42022.016	(8228)	149*	42029.773	2080	203	42032.168	812	257*	42033.204	404
96	42022.290	(8035)	150	42029.843	2043	204*	42032.195	805	258*	42033.218	393
97	42022.558	(7695)	151*	42029.911	1999	205*	42032.222	783	259*	42033.231	392
98	42022.815	(7513)	152*	42029.978	1961	206*	42032.248	778	260*	42033.244	379
99	42023.066	(7184)	153	42030.043	1918	207*	42032.274	765	261*	42033.257	383
100	42023.306	7032	154*	42030.107	1882	208*	42032.300	755	262*	42033.269	374
101	42023.539	(6931)	155*	42030.170	1851	209	42032.323	745	263*	42033.282	373
102	42023.770	(6617)	156*	42030.231	1814	210*	42032.348	733	264*	42033.294	360
103	42023.991	(6378)	157*	42030.292	1773	211*	42032.372	726	265*	42033.306	368
104	42024.204	(6294)	158*	42030.351	1738	212*	42032.397	716	266*	42033.319	359
105	42024.414	(5990)	159*	42030.409	1711	213*	42032.420	704	267*	42033.331	355
106	42024.614	5866	160	42030.466	1675	214	42032.445	689	268*	42033.342	351
107	42024.811	5704	161*	42030.522	1652	215*	42032.468	681	269*	42033.354	346
108	42025.003	5546	162	42030.577	1616	216*	42032.491	673	270*	42033.366	342
109	42025.188	(5409)	163*	42030.631	1588	217*	42032.513	664	271*	42033.377	343
110	42025.368	5251	164	42030.683	1554	218*	42032.535	651	272*	42033.389	336

TABLE I. (*Continued*).

n	Energy (cm^{-1})	$E_{n+1}-E_n$ (MHz)	n	Energy (cm^{-1})	$E_{n+1}-E_n$ (MHz)	n	Energy (cm^{-1})	$E_{n+1}-E_n$ (MHz)	n	Energy (cm^{-1})	$E_{n+1}-E_n$ (MHz)
111	42025.544	(5051)	165*	42030.735	1527	219	42032.557	648	273*	42033.400	330
112	42025.712	4960	166*	42030.786	1503	220*	42032.579	634	274*	42033.411	326
113	42025.878	4830	167*	42030.836	1470	221*	42032.600	629	275*	42033.422	324
114*	42026.039	4711	168*	42030.885	1447	222*	42032.621	617	276*	42033.432	328
115*	42026.196	4586	169*	42030.933	1420	223*	42032.641	611	277*	42033.443	317
116	42026.351	4466	170	42030.981	1396	224*	42032.662	599	278*	42033.454	307
117*	42026.500	4346	171*	42031.028	1374	225	42032.684	596	279*	42033.464	318
118	42026.645	4229	172*	42031.073	1347	226*	42032.704	591	280*	42033.475	313
119*	42026.786	4133	173*	42031.118	1325	227*	42032.724	577	281*	42033.485	283
120*	42026.924	4015	174*	42031.163	1302	228*	42032.743	573	282*	42033.495	283
121	42027.059	3934	175*	42031.206	1281	229*	42032.762	570	283*	42033.504	316
122*	42027.190	3835	176*	42031.249	1254	230	42032.777	555	284*	42033.515	283
123*	42027.318	3729	177*	42031.291	1237	231*	42032.796	551	285*	42033.524	
124	42027.442	3651	178*	42031.332	1206	232*	42032.814	546			

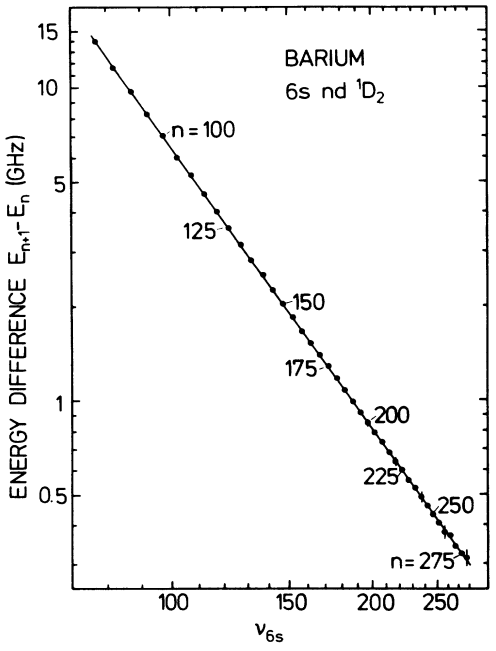

FIG. 4. Logarithmic plot of the difference $E_{n+1}-E_n$ of energies of neighboring $6snd\ ^1D_2$ Rydberg states vs effective principal quantum number ν_{6s}. Every fifth pair is plotted only. The straight line corresponds to the ν_{6s}^{-3} scaling law.

$6snd\ ^1D_2$ Rydberg states, the wavelength of the second dye laser was determined using a high-precision Michelson interferometer[48] with an accuracy of ±30 MHz. In addition, a marker cavity with a free spectral range (FSR) of 74.94(6) MHz served as a frequency scale for the second dye laser. In this way energies of $6sns\ ^1S_0$, $6snp\ ^1P_1$, and $6snd\ ^1D_2$ Rydberg states were determined by interpolating between energies measured by means of the Michelson interferometer. A spectrum of $6snd\ ^1D_2$ barium Rydberg states is shown in Fig. 3 for principal quantum numbers ranging between $n=240$ and $n=310$. The small signals which appear between the prominent

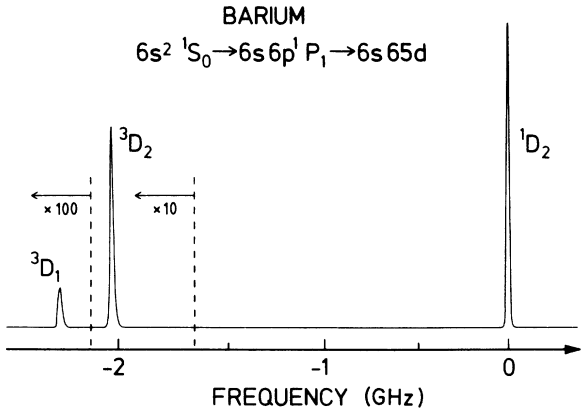

FIG. 5. Spectrum of the $6s65d\ ^{1,3}D$ fine-structure multiplet.

TABLE II. Singlet-triplet splittings $\Delta E_{ST} = E(^1D_2) - E(^3D_2)$ between $6snd\ ^{1,3}D_2$ Rydberg states of barium. Typical uncertainties are given in parentheses.

n	ΔE_{ST} (GHz)	n	ΔE_{ST} (GHz)	n	ΔE_{ST} (GHz)
30	34.416 (100)	115	0.285 (10)	136	0.183 (10)
49	5.153 (10)	116	0.281 (10)	140	0.160 (10)
50	4.832 (10)	117	0.286 (10)	145	0.146 (10)
59	2.767 (10)	118	0.272 (10)	150	0.133 (10)
60	2.648 (10)	119	0.271 (10)	155	0.119 (10)
65	2.031 (10)	120	0.262 (10)	160	0.110 (10)
81	0.962 (10)	124	0.243 (10)	165	0.099 (10)
109	0.353 (10)	127	0.215 (10)	170	0.095 (10)
113	0.314 (10)	130	0.207 (10)	180	0.079 (10)
114	0.305 (10)	133	0.190 (10)	190	0.065 (10)

TABLE III. Energies of $6sns\ ^1S_0$ ($30 \leq n \leq 214$) Rydberg states of barium. The energies were measured using a high-precision Michelson interferometer or were deduced (*) by interpolation using a marker cavity (see Table I). The overall uncertainty amounts to $\pm 0.002\ cm^{-1}$.

n	Energy (cm^{-1})	n	Energy (cm^{-1})	n	Energy (cm^{-1})	n	Energy (cm^{-1})
30	41869.958	108	42024.716	144*	42029.286	180*	42031.352
38	41938.792	109	42024.910	145*	42029.365	181*	42031.391
50	41982.561	110	42025.099	146*	42029.442	182*	42031.431
60	41999.644	111*	42025.282	147*	42029.518	183*	42031.470
61	42000.875	(112)		148*	42029.592	184*	42031.508
65	42005.206	(113)		149*	42029.667	185*	42031.545
70	42009.548	114*	42025.796	150*	42029.737	186*	42031.582
75	42013.002	115*	42025.959	151*	42029.807	187*	42031.618
80	42015.796	116*	42026.119	152*	42029.876	188*	42031.653
81	42016.291	117*	42026.273	153*	42029.943	189*	42031.689
82	42016.766	118*	42026.426	154*	42030.010	190*	42031.722
83	42017.224	119*	42026.573	155*	42030.074	191*	42031.757
84	42017.665	120*	42026.716	156*	42030.137	192*	42031.789
85	42018.089	121*	42026.855	157*	42030.200	193*	42031.822
86	42018.497	122*	42026.991	158*	42030.260	194*	42031.855
87	42018.891	123*	42027.125	159*	42030.320	195*	42031.886
88	42019.272	124*	42027.254	160*	42030.379	196*	42031.917
89	42019.636	125*	42027.380	161*	42030.437	197*	42031.948
90	42019.992	126*	42027.503	162*	42030.493	198*	42031.978
91	42020.334	127*	42027.623	163*	42030.548	199*	42032.008
92	42020.664	128*	42027.740	164*	42030.602	200*	42032.038
93	42020.983	129*	42027.852	165*	42030.656	201*	42032.066
94	42021.291	130*	42027.966	166*	42030.708	202*	42032.095
95	42021.590	131*	42028.073	167*	42030.759	203*	42032.123
96	42021.878	132*	42028.180	168*	42030.809	204*	42032.151
97	42022.158	133*	42028.283	169*	42030.859	205*	42032.181
98	42022.428	134*	42028.385	170*	42030.908	206*	42032.207
99	42022.689	135*	42028.484	171*	42030.956	207*	42032.234
100	42022.942	136*	42028.581	172*	42031.003	208*	42032.260
101	42023.188	137*	42028.676	173*	42031.050	209*	42032.286
102	42023.428	138*	42028.769	174*	42031.095	210*	42032.312
103	42023.659	139*	42028.858	175*	42031.140	211*	42032.334
104	42023.883	140*	42028.948	176*	42031.184	212*	42032.359
105	42024.101	141*	42029.036	177*	42031.227	213*	42032.383
106	42024.312	142*	42029.120	178*	42031.269	214*	42032.408
107	42024.518	143*	42029.204	179*	42031.311		

$6snd\ ^1D_2$ and $6s(n+1)d\ ^1D_2$ resonances correspond to $6s(n+2)s\ ^1S_0$ states. It should be noted that the observed linewidths exceed the natural linewidths of the Rydberg states by several orders of magnitude. Besides the finite bandwidths of the lasers, contributions arise from the residual Doppler width $\delta\nu_{res}\approx 7$ MHz of the first transition. These contributions are proportional to $\delta\nu_{res}\,|(\nu_2-\nu_1)/\nu_1|$ and result in a constant linewidth of the observed resonances in the order of a few MHz. The atomic transition frequencies of the lower and upper transitions are denoted by ν_1 and ν_2, respectively. Since the oscillator strength of the second transition decreases proportional to ν_{6s}^{-3} the amplitude of the $^1D_2$ signals are expected to decrease in the same manner with increasing effective principal quantum number ν_{6s}. However, comparing the amplitudes of the signals recorded at $n=240$ and 290, a ratio of 0.07 is deduced from the recorded spectrum whereas this ratio is expected to be larger by a factor of eight from the ν_{6s}^{-3} scaling law. This discrepancy is explained by the presence of small stray electric fields, which cause Stark mixing and hence a decrease in the $^1D_2$ signal amplitudes. It follows from a systematic investigation of the distribution of oscillator strength across Stark multiplets of barium[43] that the $6snd\ ^1D_2$ signals disappear when $3(F/F_0)n^5\approx 1$. The electric field strength F is measured in atomic units $F_0=5.14\times10^9$ V/cm. Taking $n=310$ as the principal quantum number of the highest $6snd\ ^1D_2$ resonance observed in Fig. 3, we estimate stray electric fields to be in the order of 1 mV/cm. It should be noted that further improvements of our experimental setup allowed us to reduce stray electric fields down to about 45 μV/cm. In this way $6snd\ ^1D_2$ Rydberg states with principal quantum numbers up to $n=520$ have been detected.[42]

In Table I we have listed energies of $6snd\ ^1D_2$ Ba Rydberg states for principal quantum numbers ranging between $n=30$ and 285. The energies are referred to the ground state and were obtained by adding the energy of the $6s6p\ ^1P_1$ state to the measured wave number of the second transition. We have determined the energy of the $6s6p\ ^1P_1$ level to be 18060.258(2) cm^{-1}, slightly lower than the value given in Ref. 49. The uncertainty of ±0.0015 cm^{-1} for the first and second transition results in an uncertainty of ±0.002 cm^{-1} (±60 MHz) for the energies listed in Table I. It should be noted that these values are generally smaller by 0.1–0.15 cm^{-1} compared to the values reported by Aymar *et al.*[2] Besides energies, we have measured the frequency separation $\Delta E=E_{n+1}-E_n$ between neighboring $6s(n+1)d$ and $6snd\ ^1D_2$ Rydberg states with a precision of about ±10 MHz. These energy separations may be used to identify the principal quantum numbers of $6snd\ ^1D_2$ Rydberg states without measuring their energies directly. Energy separations given in parentheses in Table I are less accurate by an order of magnitude. Figure 4 is a logarithmic plot of the frequency separation ΔE versus the effective principal quantum number ν_{6s}. For clarity, only every fifth pair has been plotted. The separation between neighboring Rydberg states scales according to ν_{6s}^{-3}, indi-

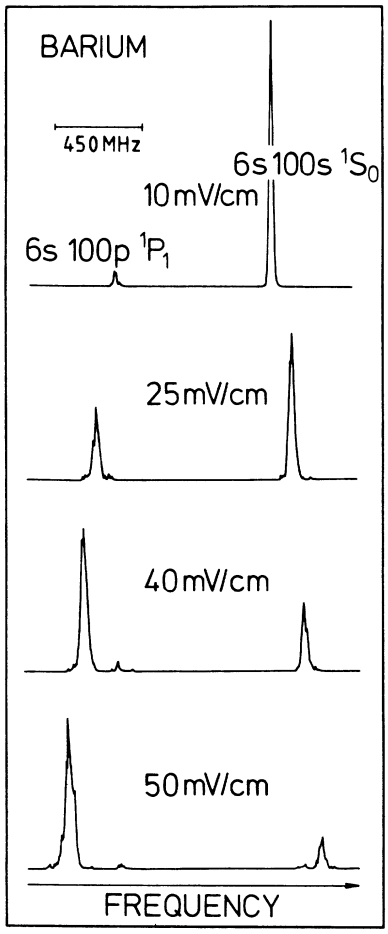

FIG. 6. Stark mixing between $6s100p\ ^1P_1$ and $6s100s\ ^1S_0$ Rydberg states. The excitation scheme shown in Fig. 1(a) was employed.

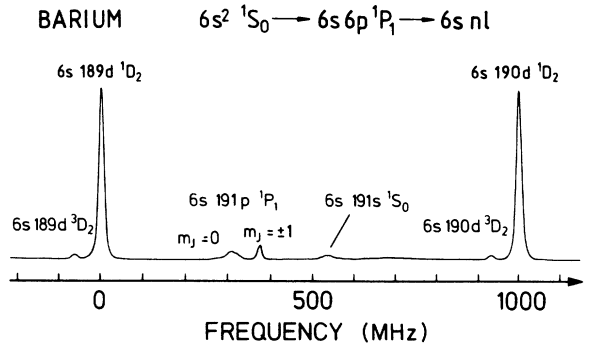

FIG. 7. Stark shifts and broadening of $6s191s\ ^1S_0$ and $6s191p\ ^1P_1$ ($m=0$) Rydberg levels due to stray electric fields. The position of the $m=\pm1$ components corresponds to the energy of the $6s191p\ ^1P_1$ state in zero field. The shift of the $6s191s\ ^1S_0$ state from its zero field position towards higher energies equals the splitting between the $6s191p\ ^1P_1$, $m=0$ and $m=\pm1$ components.

cating that the $6snd\ ^1D_2$ Rydberg series is not perturbed by doubly excited states in this energy range.

We have used those energies of $6snd\ ^1D_2$ Rydberg states, which have been measured by means of the high-precision Michelson interferometer to derive the first ionization limit I_{6s} of barium. Energies marked by an asterisk in Table I were interpolated by means of a marker cavity and hence have not been considered for the determination of I_{6s}. Using a simple Rydberg formula and energies of $6snd\ ^1D_2$ Rydberg states with $78 \leq n \leq 230$ we obtain for the first ionization limit $I_{6s} = 42\,034.902(3)$ cm^{-1}. Lower-lying Rydberg states ($n < 78$) have been excluded because of the perturbation of the $6snd\ ^1D_2$ Rydberg series by the $5d7d\ ^1D_2$ state, located between $n = 26$ and 27. Furthermore, a three channel quantum defect model, which accounts for the configuration interaction of the $5d7d\ ^1D_2$ perturber and the $6snd\ ^1D_2$, $6snd\ ^3D_2$ Rydberg series, leads to the same value for the ionization limit.

Besides energies of $6snd\ ^1D_2$ Rydberg states we report the singlet-triplet splitting between $^1D_2$ and $^3D_2$ Rydberg states (Table II). A typical spectrum used to derive singlet-triplet splittings is shown in Fig. 5, displaying the $6s65d\ ^3D_1$, $^3D_2$, and $^1D_2$ fine-structure components. In order to excite the $^3D_1$ state, the angle between the polarization vectors of both linearly polarized laser beams was chosen to be 45°.

Energies of $6sns\ ^1S_0$ Rydberg states are listed in Table III for principal quantum numbers ranging between $n = 30$ and 214. Energies of $6sns\ ^1S_0$ Rydberg states ($n \leq 61$) reported previously by Aymar *et al.*[2] are generally lower by 0.1–0.15 cm^{-1}. In addition we have determined energies of $6snp\ ^1P_1$ Rydberg states ($60 \leq n \leq 214$) which are given in Table IV. Below $n = 100$ we have measured the frequency separation between $6sns\ ^1S_0$ and $6snp\ ^1P_1$ ($m = 0$) states as a function of the electric field strength applied. By extrapolating to zero electric field and using energies of $6sns\ ^1S_0$ states, the data in Table IV were derived. Figure 6 illustrates the repulsion of neighboring $6s100p\ ^1P_1$ ($m = 0$) and $6s100s\ ^1S_0$ Rydberg states. Because of Stark mixing the relative intensities of the recorded signals change dramatically on varying the external electric field strength. At principal quantum numbers well above $n = 100$, stray electric fields are sufficient to cause considerable second-order Stark shifts and broadening because of the near degeneracy of the $6sns\ ^1S_0$ and $6snp\ ^1P_1$ ($m = 0$) Rydberg states. The repulsion of the $6s191s\ ^1S_0$ and $6s191p\ ^1P_1$ ($m = 0$) Rydberg states caused by stray electric fields is illustrated in Fig. 7. On the contrary, the Stark shifts ex-

TABLE IV. Energies of $6snp\ ^1P_1$ ($60 \leq n \leq 214$) Rydberg states of barium. The overall uncertainty amounts to ± 0.002 cm^{-1}. The energies were derived from recorded spectra using a marker cavity and the data given in Tables I and III.

n	Energy (cm^{-1})	n	Energy (cm^{-1})	n	Energy (cm^{-1})	n	Energy (cm^{-1})
60*	41999.637	129*	42027.840	158*	42030.254	187*	42031.614
61*	42000.860	130*	42027.954	159*	42030.314	188*	42031.649
65*	42005.177	131*	42028.061	160*	42030.373	189*	42031.685
70*	42009.511	132*	42028.168	161*	42030.431	190*	42031.719
75*	42012.963	133*	42028.273	162*	42030.487	191*	42031.754
80*	42015.758	134*	42028.374	163*	42030.543	192*	42031.786
85*	42018.054	135*	42028.474	164*	42030.597	193*	42031.819
90*	42019.960	136*	42028.571	165*	42030.651	194*	42031.852
95*	42021.559	137*	42028.666	166*	42030.703	195*	42031.884
100*	42022.915	138*	42028.759	167*	42030.754	196*	42031.915
108*	42024.692	139*	42028.849	168*	42030.805	197*	42031.945
109*	42024.887	140*	42028.940	169*	42030.854	198*	42031.975
110*	42025.076	141*	42029.027	170*	42030.903	199*	42032.005
111*	42025.259	142*	42029.111	171*	42030.951	200*	42032.035
114*	42025.777	143*	42029.196	172*	42030.999	201*	42032.064
115*	42025.941	144*	42029.278	173*	42031.045	202*	42032.093
116*	42026.101	145*	42029.357	174*	42031.090	203*	42032.121
117*	42026.256	146*	42029.434	175*	42031.134	204*	42032.148
118*	42026.409	147*	42029.510	176*	42031.179	205*	42032.178
119*	42026.556	148*	42029.585	177*	42031.222	206*	42032.205
120*	42026.700	149*	42029.659	178*	42031.265	207*	42032.232
121*	42026.840	150*	42029.730	179*	42031.306	208*	42032.258
122*	42026.976	151*	42029.799	180*	42031.347	209*	42032.284
123*	42027.110	152*	42029.869	181*	42031.387	210*	42032.310
124*	42027.240	153*	42029.936	182*	42031.427	211*	42032.333
125*	42027.366	154*	42030.003	183*	42031.465	212*	42032.357
126*	42027.489	155*	42030.067	184*	42031.504	213*	42032.381
127*	42027.610	156*	42030.131	185*	42031.541	214*	42032.406
128*	42027.727	157*	42030.194	186*	42031.578		

perienced by $6snp\ ^1P_1$ ($m=\pm1$) components cancel in first approximation because $6snp\ ^1P_1$ levels lie approximately halfway between the neighboring $6s(n-2)d$ and $6s(n-1)d\ ^1D_2$ ($m=\pm1$) Rydberg states (see Fig. 7). However, the Stark mixing of the $6snp\ ^1P_1$ ($m=\pm1$) components with the neighboring $^1D_2$ states results in an increase in oscillator strength of the $6s6p\ ^1P_1 \rightarrow 6snp\ ^1P_1$ ($m=\pm1$) transition. It follows that the energy of the $6s191p\ ^1P_1$ state in zero electric field can be inferred immediately from the spectrum shown in Fig. 7. Furthermore, the frequency separation between the $6s191p\ ^1P_1$ $m=0$ and $m=\pm1$ components is equal to the Stark shift experienced by the $6s191s\ ^1S_0$ state. Correcting for this shift the energies of $6sns\ ^1S_0$ Rydberg states at high principal quantum numbers were obtained. The data given in Tables I, III, and IV are summarized in Fig. 8, where we have plotted the effective principal quantum number ν_{6s} (modulo 1) for $6sns\ ^1S_0$, $6snp\ ^1P_1$, and $6snd\ ^1D_2$ Rydberg states versus the principal quantum number n. Starting at $n=50$, the principal quantum number increases in steps of 5. Using the ionization limit $I_{6s}=42\,034.902$ cm^{-1} the effective principal quantum number ν_{6s} (modulo 1), is constant within our accuracy for $6sns\ ^1S_0$ and $6snd\ ^1D_2$ Rydberg states with $n\geq60$ and $n\geq78$, respectively. On the contrary, the effective principal quantum number of the $6snp\ ^1P_1$ series is seen to vary below $n<100$. This variation is caused by the configuration interaction with the $5d8p\ ^1P_1$ state, straddling the ionization limit.[3] Because of this perturbation, all $6snp\ ^1P_1$ Rydberg states are pushed towards lower energies. Therefore $6snp\ ^1P_1$ states lie below the corresponding $6sns\ ^1S_0$ levels for $n\geq60$, while the opposite is true for $n\leq58$ (see Tables III and IV and Figs. 6, 7, and 8). The horizontal straight lines, shown in Fig. 8, correspond to the (limiting) values for the quantum defects δ_l with $\delta_0(n\geq50)=4.212(5)$, $\delta_1(n\geq100)=4.332(5)$, and $\delta_2(n\geq78)=2.718(5)$.

Apart from energies of $6sns\ ^1S_0$, $6snp\ ^1P_1$, and $6snd\ ^{1,3}D_2$ Rydberg states, we have measured those of

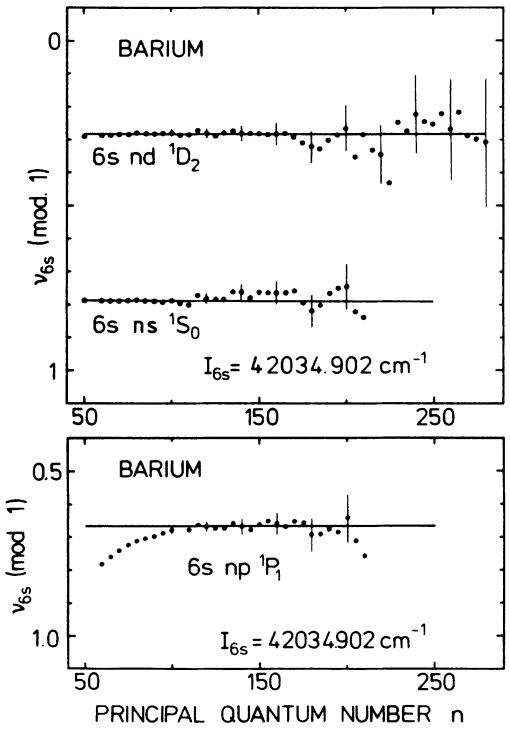

FIG. 8. Effective principal quantum number ν_{6s} (modulo 1) vs principal quantum number. The solid lines correspond to the limiting values of the quantum defects δ_l of the $^1S_0$, $^1P_1$, and $^1D_2$ series, given in the text. The deviations observed for the $6snp\ ^1P_1$ states below $n=100$ are caused by the $5d8p\ ^1P_1$ perturbing state.

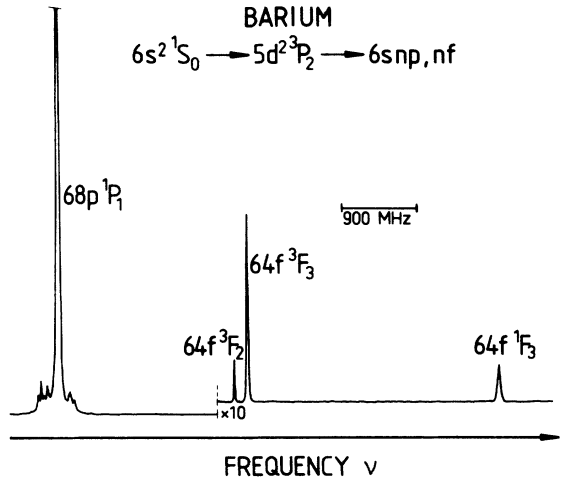

FIG. 9. Spectrum of the $6s64f\ ^{1,3}F$ fine-structure multiplet in the vicinity of the $6s68p\ ^1P_1$ state.

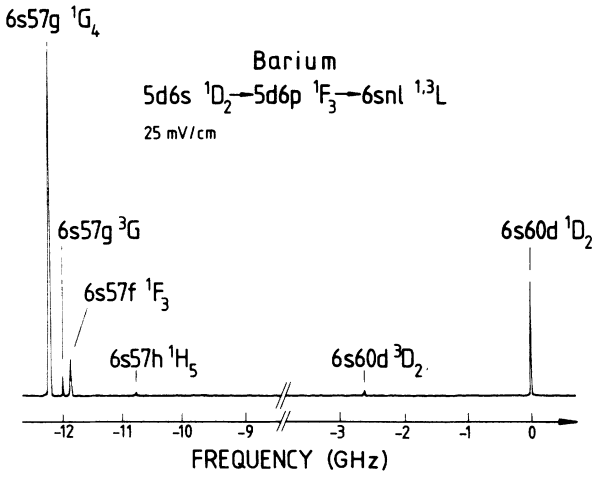

FIG. 10. Spectrum of the $6s57f\ ^1F_3$, $57g\ ^1G_4$, and $57h\ ^1H_5$ Rydberg states of barium. The energies are measured with respect to the nearest $(6s60d)\ ^1D_2$ state. The total angular momentum of the $57g\ ^3G$ state is unknown. A small electric field was applied in order to excite odd parity states.

TABLE V. Energies of $6snf\ ^1F_3$, $^3F_2$, $^3F_3$, $6sng\ ^1G_4$, $6sng\ ^3G$, and $6snh\ ^1H_5$ Rydberg states of barium ($47 \leq n \leq 78$). The overall accuracy amounts to ± 0.002 cm^{-1}. The energies were deduced from recorded spectra using a marker cavity and the data given in Tables I, III, and IV.

Level	Energy (cm^{-1})	Level	Energy (cm^{-1})	Level	Energy (cm^{-1})	Level	Energy (cm^{-1})
$6s47f\ ^1F_3$	41985.132	$6s67f\ ^3F_2$	42010.327	$6s57g\ ^1G_4$	42001.059	$6s72g\ ^3G$	42013.702
$6s57f\ ^1F_3$	42001.069	$6s67f\ ^3F_3$	42010.332	$6s62g\ ^1G_4$	42006.300	$6s75g\ ^3G$	42015.367
$6s61f\ ^3F_2$	42005.241	$6s67f\ ^1F_3$	42010.418	$6s67g\ ^1G_4$	42010.412	$6s76g\ ^3G$	42015.878
$6s61f\ ^3F_3$	42005.247	$6s71f\ ^3F_2$	42013.024	$6s72g\ ^1G_4$	42013.696	$6s78g\ ^3G$	42016.840
$6s61f\ ^1F_3$	42005.364	$6s71f\ ^3F_3$	42013.027	$6s75g\ ^1G_4$	42015.361	$6s57h\ ^1H_5$	42001.106
$6s62f\ ^3F_2$	42006.193	$6s71f\ ^1F_3$	42013.100	$6s76g\ ^1G_4$	42015.871	$6s62h\ ^1H_5$	42006.338
$6s62f\ ^3F_3$	42006.198	$6s72f\ ^1F_3$	42013.704	$6s78g\ ^1G_4$	42016.834	$6s67h\ ^1H_5$	42010.441
$6s62f\ ^1F_3$	42006.309	$6s75f\ ^1F_3$	42015.370	$6s47g\ ^3G$	41985.113	$6s72h\ ^1H_5$	42013.722
$6s66f\ ^3F_2$	42009.575	$6s76f\ ^1F_3$	42015.881	$6s57g\ ^3G$	42001.065	$6s75h\ ^1H_5$	42015.384
$6s66f\ ^3F_3$	42009.580	$6s78f\ ^1F_3$	42016.843	$6s62g\ ^3G$	42006.307	$6s76h\ ^1H_5$	42015.893
$6s66f\ ^1F_3$	42009.670	$6s47g\ ^1G_4$	41985.103	$6s67g\ ^3G$	42010.416	$6s78h\ ^1H_5$	42016.854

$6snf\ ^{1,3}F$, $6sng\ ^{1,3}G$, and $6snh\ ^1H_5$ states (see Table V) for principal quantum numbers between $n=47$ and 78. Starting from the $5d^2\ ^3P_2$ intermediate level [Fig. 1(c)] $6snp\ ^1P_1$ and $6snf\ ^{1,3}F$ Rydberg states can be excited because of configuration mixing present in the intermediate and final (Rydberg) states. In particular, $6snp\ ^1P_1$ Rydberg states contain some $5d8p\ ^1P_1$ character, as discussed above. Energies of $6snf\ ^1F_3$, $^3F_{2,3}$ Rydberg states were derived from spectra such as the one shown in Fig. 9. For this purpose we have measured frequency separations between signals corresponding to $6s(n+4)p\ ^1P_1$ and $6snf\ ^1F_3$, $^3F_{2,3}$ states using a marker cavity with a FSR of 149.53(18) MHz. Energies of $6snf\ ^1F_3$, $^3F_{2,3}$ Rydberg states were derived from the measured frequency separations and the energies of $6s(n+4)p\ ^1P_1$ states given in Table IV. We have compared our data with energies of $6snf$ Rydberg states at lower ($n=45-55$) principal quantum numbers by calculating the corresponding quantum defects. Excellent agreement with the data reported by Post *et al.*[8] was found.

In Fig. 10 we show a spectrum of $6s57g\ ^{1,3}G$ and $6s57h\ ^1H_5$ Rydberg states excited via the $5d6p\ ^1F_3$ intermediate level. In order to reach odd parity states, an electric field of 25 mV/cm had been applied while recording this spectrum. The signals were identified on account of their quantum defects, their intensities and their behavior on application of small electric fields ($F \lesssim 400$ mV/cm). For example, the frequency separation between the $6s60d\ ^1D_2$ and $6s57f\ ^1F_3$ Rydberg states is known from our experiments discussed in the previous paragraphs. It is obtained from the splittings between the Rydberg states $6s60d\ ^1D_2-6s61s\ ^1S_0$, $6s61s\ ^1S_0-6s61p\ ^1P_1$, and $6s61p\ ^1P_1-6s57f\ ^1F_3$, measured separately with an accuracy of ± 10 MHz. The $60d\ ^1D_2-57f\ ^1F_3$ frequency separation, derived in this way, is in excellent agreement with the splitting observed in Fig. 10. Furthermore, the strongest signal appearing in Fig. 10 is readily identified as $6s57g\ ^1G_4$ state. Because of their near degeneracy, the $6s57g\ ^1G_4$ and $6s57f\ ^1F_3$ states are strongly coupled by small external fields allowing the $^1F_3$ state to be observed in fields as low as 25 mV/cm. On the other hand, Stark mixing between the $6s57f\ ^1F_3$ and $6s60d\ ^1D_2$ states can be neglected at this field strength because of their large frequency separation. Similar arguments can be used to justify the identification of the $6s57h\ ^1H_5$ state. This resonance is not observed in

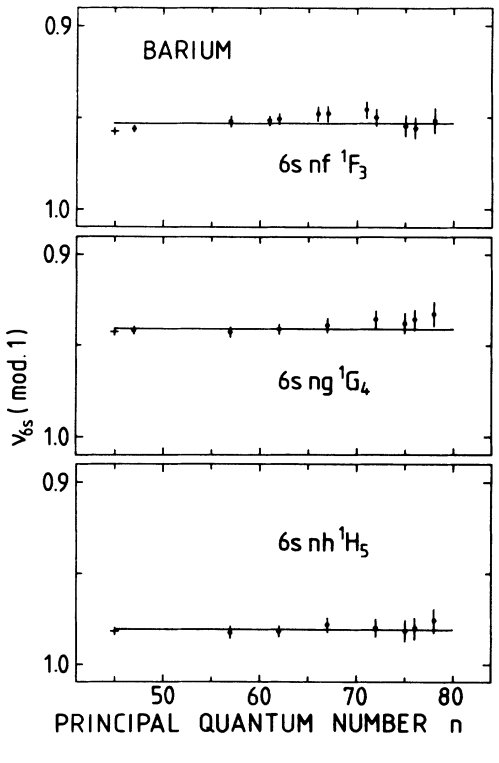

FIG. 11. Effective principal quantum numbers ν_{6s} (modulo 1) vs principal quantum number. The solid lines correspond to the limiting values of the quantum defects δ_l of the $^1F_3$, $^1G_4$, and $^1H_5$ states given in the text. The data marked by a cross (+) were taken from Refs. 8 and 9.

zero electric field. From similar spectra taken for different principal quantum numbers, we have derived the energies of $6snf\ ^1G_4$, $6sng\ ^3G$, and $6snh\ ^1H_5$ states listed in Table V. The total angular momentum quantum number J of the ^3G states is unknown.

In Fig. 11, we have plotted the effective principal quantum number ν_{6s} (modulo 1) of $6snf\ ^1F_3$, $6sng\ ^1G_4$, and $6snh\ ^1H_5$ Rydberg states versus principal quantum number n. Within experimental error no variations are observed for principal quantum numbers ranging between $n=47$ and 78. The solid lines correspond to the average values $\delta_3=0.047$, $\delta_4=0.059$, and $\delta_5=0.019$. These values are consistent with quantum defects derived from energies of $^1F_3$, $^1G_4$, and $^1H_5$ Rydberg states of barium at lower principal quantum numbers.[8,9]

In summary, we have measured energies of high-n Ba Rydberg states ($30 \leq n \leq 285$, $0 \leq l \leq 5$) with an uncertainty of ± 0.002 cm^{-1}. In addition, the energy differences $E_{n+1}-E_n$ between neighboring $6snd\ ^1D_2$ Rydberg states have been determined up to ± 10 MHz. These data can be exploited to determine the principal quantum numbers of high-lying barium Rydberg states. Energy separations between neighboring Rydberg states, deduced from a series of recorded resonances, allow to deduce the principal quantum numbers without measuring the absolute energies of the states with high precision.

This work was supported by the Deutsche Forschungsgemeinschaft, Sonderforschungsbereich 161. We thank Professor Dr. Welgehausen and Dr. Frölich for loan of the Michelson interferometer.

*Present address: Physikalisch-Technische Bundesanstalt, Abbestrasse 2-12, 1000 Berlin 10, West Germany.

†Present address: Department of Physics, Lund Institute of Technology, P.O. Box 118, S-22100 Lund, Sweden.

‡Present address: Krone G.m.b.H., Goerzallee 311, 1000 Berlin 37, West Germany.

[1]J. R. Rubbmark, S. A. Borgström, and K. Bockasten, J. Phys. B **10**, 421 (1977).

[2]M. Aymar, P. Camus, M. Dieulin, and C. Morillon, Phys. Rev. A **18**, 2173 (1978).

[3]J. A. Armstrong, J. J. Wynne, and P. Esherick, J. Opt. Soc. Am. **69**, 211 (1979).

[4]M. Aymar and O. Robaux, J. Phys. B **12**, 531 (1979).

[5]P. Camus, M. Dieulin, and A. El Himdy, Phys. Rev. A **26**, 379 (1982).

[6]M. Aymar and P. Camus, Phys. Rev. A **28**, 850 (1983).

[7]B. H. Post, W. Hogervorst, and W. Vassen, Phys. Rev. A **29**, 2989 (1984).

[8]B. H. Post, W. Vassen, W. Hogervorst, M. Aymar, and O. Robaux, J. Phys. B **18**, 187 (1985).

[9]W. Vassen, E. Bente, and W. Hogervorst, J. Phys. B **20**, 2383 (1987).

[10]D. Kaiser, P. Kulina, A. E. Livingston, H.-H. Radloff, and S. Tudorache, Z. Phys. A **285**, 111 (1978).

[11]M. Aymar, R.-J. Champeau, C. Delsart, and J.-C. Keller, J. Phys. B **14**, 4489 (1981).

[12]K. Bhatia, P. Grafström, C. Levinson, H. Lundberg, L. Nilsson, and S. Svanberg, Z. Phys. A **303**, 1 (1981).

[13]T. F. Gallagher, W. Sandner, and K. A. Safinya, Phys. Rev. A **23**, 2969 (1981).

[14]M. Aymar, P. Grafström, C. Levinson, H. Lundberg, and S. Svanberg, J. Phys. B **15**, 877 (1982).

[15]J. Neukammer, E. Matthias, and H. Rinneberg, Phys. Rev. A **25**, 2426 (1982).

[16]H. Rinneberg, J. Neukammer, and E. Matthias, Z. Phys. A **306**, 11 (1982).

[17]P. Grafström, J. Zhan-Kui, G. Jönsson, S. Kröll, C. Levinson, H. Lundberg, and S. Svanberg, Z. Phys. A **306**, 281 (1982).

[18]H. Rinneberg and J. Neukammer, Phys. Rev. Lett. **49**, 124 (1982).

[19]J. Neukammer and H. Rinneberg, J. Phys. B **15**, L425 (1982).

[20]H. Rinneberg and J. Neukammer, J. Phys. B **15**, L825 (1982).

[21]E. R. Eliel and W. Hogervorst, J. Phys. (Paris) Colloq. **43**, C2-443 (1982).

[22]J. Neukammer and H. Rinneberg, J. Phys. B **15**, 3787 (1982).

[23]J. Neukammer and H. Rinneberg, J. Phys. B **15**, L723 (1982).

[24]H. Rinneberg and J. Neukammer, Phys. Rev. A **27**, 1779 (1983).

[25]W. Hogervorst and E. R. Eliel, Z. Phys. A **310**, 19 (1983).

[26]E. R. Eliel and W. Hogervorst, J. Phys. B **16**, 1881 (1983).

[27]H. Rinneberg and J. Neukammer, J. Phys. (Paris) Colloq. **44**, C7-177 (1983).

[28]E. R. Eliel and W. Hogervorst, Phys. Rev. A **27**, 2995 (1983).

[29]B. H. Post, W. Vassen, and W. Hogervorst, J. Phys. B **19**, 511 (1986).

[30]M. L. Zimmerman, T. W. Ducas, M. G. Littman, and D. Kleppner, J. Phys. B **11**, L11 (1978).

[31]K. A. H. van Leeuwen, W. Hogervorst, and B. H. Post, Phys. Rev. A **28**, 1901 (1983).

[32]P. Kulina and R.-H. Rinkleff, Z. Phys. A **318**, 251 (1984).

[33]M. A. Zaki Ewiss, W. Hogervorst, W. Vassen, B. H. Post, and H. Wijnen, Z. Phys. A **322**, 385 (1985).

[34]P. Grafström, C. Levinson, H. Lundberg, S. Svanberg, P. Grundevik, L. Nilsson, and M. Aymar, Z. Phys. A **308**, 95 (1982).

[35]C. W. Clark, K. T. Lu, and A. F. Starace, *Progress in Atomic Spectroscopy,* edited by H.-J. Beyer and H. Kleinpoppen (Plenum, New York, 1984), Pt. C, p. 247.

[36]H.-J. Grabka, M. Kohl, K. Vietzke, J. Neukammer, and H. Rinneberg (unpublished).

[37]W. Hogervorst, Comments At. Mol. Phys. **13**, 69 (1983).

[38]M. Aymar, J. Opt. Soc. Am. B **1**, 239 (1984).

[39]M. Aymar, Phys. Rep. **110**, 163 (1984).

[40]H. Rinneberg, *Progress in Atomic Spectroscopy,* edited by H.-J. Beyer and H. Kleinpoppen (Plenum, New York, 1987), Pt. D, p. 157.

[41]H. Rinneberg, J. Neukammer, G. Jönsson, H. Hieronymus, A. König, and K. Vietzke, Phys. Rev. Lett. **55**, 382 (1985).

[42]J. Neukammer, H. Rinneberg, K. Vietzke, A. König, H. Hieronymus, M. Kohl, H.-J. Grabka, and G. Wunner, Phys. Rev. Lett. **59**, 2947 (1987).

[43]H. Rinneberg, J. Neukammer, A. König, K. Vietzke, H. Hieronymus, M. Kohl, H.-J. Grabka, and G. Jönsson, *Laser Spectroscopy VIII,* edited by W. Persson and S. Svanberg, (Springer-Verlag, Berlin, 1987), p. 183.

[44]H. Rinneberg, J. Neukammer, M. Kohl, A. König, K.

Vietzke, H. Hieronymus, and H.-J. Grabka, *Atomic Excitation and Recombination in External Fields II,* edited by C. W. Clark and H. S. Taylor (Plenum, New York, in press).
[45]K. C. Harvey, Rev. Sci. Instrum. **52**, 204 (1981).
[46]R. Beigang, W. Makat, and A. Timmermann, Opt. Commun. **49**, 253 (1984).
[47]H. Rinneberg, J. Neukammer, U. Majewski, and G. Schönhense, Phys. Rev. Lett. **51**, 1546 (1983).
[48]R. Beigang, K. Lücke, A. Timmermann, P. J. West, and D. Frölich, Opt. Commun. **42**, 19 (1982).
[49]C. E. Moore, *Atomic Energy Levels,* Natl. Bur. Stand. (U.S.) Circ. No. 467 (U.S. GPO, Washington, D.C., 1958).